LAWRENCE
LIVERMORE
NATIONAL
LABORATORY

LLNL-CONF-415198

Advances in Optical Fiber-Based Faraday Rotation Diagnostics

A. D. White, G. B. McHale, D. A. Goerz

July 31, 2009

17th IEEE International Pulsed Power Conference
Washington DC, DC, United States
June 29, 2009 through July 2, 2009

Disclaimer

Advances in Optical Fiber-Based Faraday Rotation Diagnostics*

A.D. White, G.B. McHale, D.A. Goerz
Lawrence Livermore National Laboratory, PO Box 808, L-153
Livermore, CA 94550, USA

Abstract

In the past two years, we have used optical fiber-based Faraday Rotation Diagnostics (FRDs) to measure pulsed currents on several dozen capacitively driven and explosively driven pulsed power experiments. We have made simplifications to the necessary hardware for quadrature-encoded polarization analysis, including development of an all-fiber analysis scheme. We have developed a numerical model that is useful for predicting and quantifying deviations from the ideal diagnostic response. We have developed a method of analyzing quadrature-encoded FRD data that is simple to perform and offers numerous advantages over several existing methods. When comparison has been possible, we have seen good agreement with our FRDs and other current sensors.

I. INTRODUCTION

The Faraday effect is a magneto-optical effect that produces a rotation of the plane of polarization of light passing through magnetized media. This effect has been exploited on pulsed power experiments for over 40 years to provide measurements of both current and magnetic field. FRDs measure the induced rotation of light traveling through a sensing medium, which can be related to the current or magnetic field in the sensing region.

Diagnostics based on the Faraday effect offer a number of advantages over conventional inductive field-sensing diagnostics. The sensing medium itself in Faraday sensors is entirely dielectric and so poses minimal risk to perturbation of the experiment, and is nearly immune to EMI. The bandwidth of Faraday effect sensors is limited by the optical transit time through the sensing medium, and linearity is excellent, especially in diamagnetic sensing media (e.g., fused-silica based optical fiber). The mechanism through which fields are measured is drastically different than inductive coupling; implementing both types of sensor provides valuable redundancy on single-shot high-value experiments. The required signal processing of the digitized data is minimal, and no integration is required unlike in many inductive field probes.

II. POLARIZATION EVOLUTION IN TWISTED SINGLE-MODE FIBER

The evolution of the state-of-polarization in optical fibers is a topic that has been well covered in other literature [1] [2] [3]. We will only restate the results here that are necessary for an understanding of our application.

Faraday rotation is a type of circular birefringence—an effect that produces different velocities of propagation for left- and right-handed circularly polarized light. Since any state-of-polarization can be decomposed into left- and right-handed circular components, Faraday rotation manifests itself in the rotation of the plane-of-polarization of light passing through magnetized media. For optical fiber sensors looped around a current carrying conductor, the magnitude of the rotation is given by:

$$\beta = V \int_0^L \vec{B} d\vec{l} = \mu V N I, \qquad (1)$$

where μV is the Verdet constant in rad/A, N is the number of fiber loops, and I is the current flowing through the loop. This is illustrated in Fig. 1. The Faraday effect is nonreciprocal; light that is reflected from the end of a Faraday sensor and passes back through the sensing region will have twice the induced rotation of light that passes through the sensing region a single time. The direction of rotation is described by the sign on the Verdet constant—a positive Verdet constant implies right-handed rotation of the plane-of-polarization relative to the magnetic field, as shown in Figs. 1 and 2.

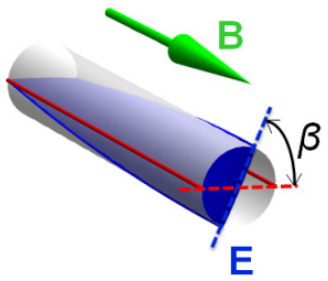

Figure 1. Graphical illustration of the Faraday effect. The plane-of-polarization E of light traveling down a fiber is rotated through an angle β due to the longitudinal magnetic field B.

* This work performed under the auspices of the U.S. Department of Energy by Lawrence Livermore National Laboratory under Contract DE-AC52-07NA27344.

Most stresses in single mode fiber result in linear birefringence, or a difference in velocity of propagation for orthogonal components of linearly polarized light. The most common sources of stress we encounter are core ellipticity and other intrinsic stresses built into the fiber, and externally applied stresses from pinching, bending, or clamping.

The interaction between linear and circular birefringences are complex [1] but can be summarized by stating that that the larger effect will tend to dominate. It is therefore critical to minimize linear birefringence in the sensing region of a FRD.

One straightforward way to accomplish this is to physically twist the optical fiber. Doing so creates a small amount of circular birefringence in the optical fiber, which has the effect of causing the plane-of-polarization to rotate within the fiber.

The rate at which the plane-of-polarization rotates is described by:

$$\gamma = g\tau \qquad (2)$$

where γ is the rate of rotation of the plane-of-polarization in rad/m, τ is the twist rate in rad/m, and g is a unitless material parameter. By forcing the plane-of-polarization to rotate as it travels along the fiber, the effect of neither intrinsic birefringence nor bend-induced birefringence will accumulate with length—since the axes along which these effects act are rotating relative to the plane-of-polarization, the effects of the linear birefringences tend to average out rather than accumulate. We have measured g up to a twist rate of 400 rad/m to be 0.073 in Corning HI 780 at 850 nm, which is in good agreement with theory [2].

With an applied magnetic field, the rotation induced by twisting will sum with the rotation produced by the Faraday effect. Care should be taken to determine if at some anticipated magnetic field level, the combination of Faraday- and twist-induced rotation will cause the axes of the plane-of-polarization to align with the intrinsic fiber axes or the bend axis of the fiber loop. In the former case, intrinsic birefringence will accumulate, which can severely affect the measured rotation for long or particularly birefringent fibers. In the latter case, bend-induced birefringence will accumulate, which can severely affect the data for tightly wound sensor coils.

Fig. 2 illustrates the interaction between Faraday induced and twist induced rotation.

In Fig. 2a) the fiber is untwisted with no magnetic field applied. In this configuration, both intrinsic and bend-induced birefringence will accumulate. In Fig. 2b), a twist is imparted to the fiber, and a rotation is induced in the plane-of-polarization of light propagating along the fiber. In Fig. 2c) a small magnetic field is applied in the direction indicated. At a relatively low field level, the plane-of-polarization will re-align with the lab frame (the image frame), causing bend-induced birefringence to accumulate. In Fig. 2d) the magnetic field is increased; for all values of magnetic field larger than that in Fig. 2c), no alignment with birefringent axes will take place with this orientation of magnetic field. In Fig. 2e), the direction of the magnetic field is reversed; at low levels, the plane-of-polarization does not align with any birefringent axes. In Fig. 2f), the amplitude of the magnetic field is increased, and the plane-of-polarization aligns with the untwisted fiber axes, causing intrinsic birefringence to accumulate along the length of the fiber.

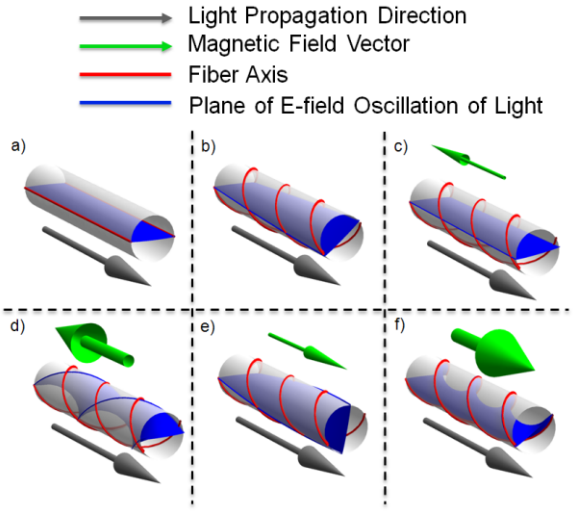

Figure 2. Illustration of interaction between twist and Faraday induced rotation. Magnetic field vector is on top of fiber; size scales with amplitude. A vector indicating direction of light propagation is shown below the fiber.

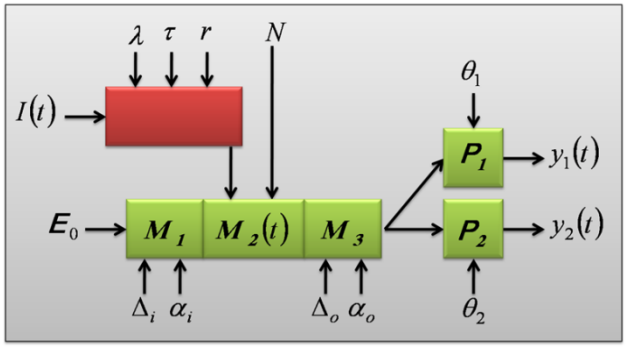

Figure 3. Block diagram of numerical model.

Intelligent choice of the direction of propagation of light in a sensor can often prevent the accumulation of linear birefringence, but this is not always the case. For very large magnetic fields, or bi-polar magnetic fields, the twist and Faraday induced rotation may inevitably cause the plane-of-polarization to align with one of the birefringent axes regardless of twist rate and choice of propagation direction. In such scenarios, we use a numerical model to estimate the effect of such birefringences on the sensor output, and select design parameters that minimize this effect.

The numerical model was formed by combining Jones' calculus matrices for the various optical elements in an FRD. A block diagram of the model is shown in Fig. 3. Model inputs are indicated by arrows pointing inwards, and outputs with arrows pointing outwards.

The Jones' matrix for the sensor fiber combines the effects of linear and circular birefringence, the mathematics of which has been derived by others [1]. The circular birefringence in the sensor fiber is a combination of twist-induced and Faraday-induced rotation, and is computed from a user-defined twist rate, a user-defined current waveform, and a user-defined wavelength. The linear birefringence in the sensor element is computed from user-defined intrinsic birefringence and computed bend birefringence. The bend-induced birefringence is calculated based on the user-defined bend radius of the sensor fiber, using models derived by others [2].

The Jones' matrix elements for the remaining model elements are straightforward and can be found in many optics texts [4]. Elements M_1 and M_3 are linear retarders at the input and output to the sensing region, representing untwisted fiber leads, with retardations Δ_i and Δ_o and fast axes at angles α_i and α_o. Elements P_1 and P_2 combine the effects of polarizers and photodetectors, with the polarizers at angles θ_1 and θ_2. The outputs of the photodetectors, y_1 and y_2 are scaled photodetector voltages and are the outputs of the model.

An example of model output is shown in Fig. 4. The inputs for this example were as follows: $N = 1$ loop of fiber with radius 20 cm, $\lambda = 850$ nm, twist rate $\tau = 10$ twists/m, 1 rad of retardation at the input and output with fast axes at angles of $-\pi/4$ rad and 0 rad respectively, polarizers at relative 45°, and a current waveform shown in Fig. 4. Light is propagating in the same direction as the magnetic field in this example.

The ideal Lissajous is a circle with a diameter of 1 V. The retardation at the input and output cause the Lissajous to distort into the ellipse seen in Fig. 4. At a current of around 29.7 MA, the magnetic field causes the plane-of-polarization to align with the original untwisted fiber axes, causing linear birefringence in the sensing region to affect the measured Faraday rotation. This results in the distortion of the Lissajous figure seen in Fig. 4 between $t = 35$ µs and $t = 45$ µs. Propagating light in the opposite direction—against the direction of the pulsed magnetic field—causes the bend-induced birefringence to affect the data at a much lower current (~2.3 MA), but to such a minor degree it can be considered unnoticeable. We have verified experimentally similar results using sensor fibers in explosive flux compression generators.

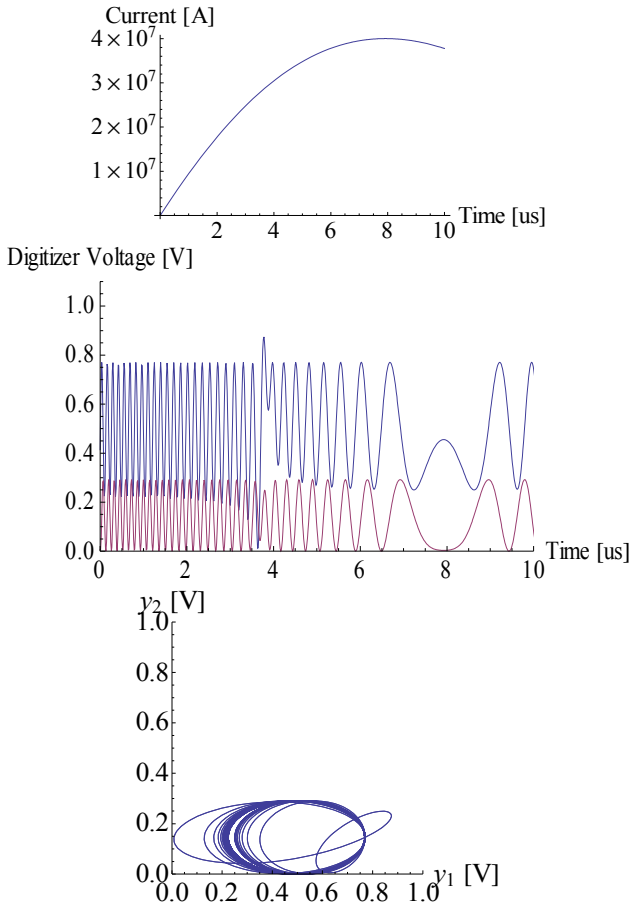

Figure 4. Example of numerical model output; input current waveform (top), quadrature-encoded photodetectors responses (middle) and Lissajous figure (bottom)

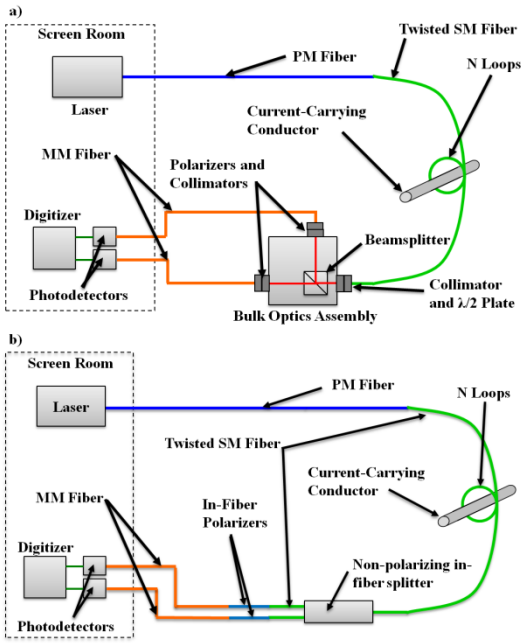

Figure 5. Typical FRD implementation, using a) bulk optics analysis and b) all-fiber analysis

III. EXPERIMENTAL RESULTS

We have implemented FRDs on dozens of capacitively driven and explosively driven pulsed power experiments over the past two years. We have used both 635 nm and 850 nm light, and observed good agreement with other diagnostics.

A. Implementation

We began implementing our diagnostics using the setup shown in Fig 5a). The analysis hardware uses collimators and free-space optics to achieve the beam-splitting and polarizing necessary for quadrature-encoded data, or photodetector signals that are 90° out of phase.

We have developed an alternative method of achieving quadrature-encoded data by using only in-fiber components. The performance is very similar to the free-space optics solution, but with lower component cost and easier assembly. We have built and tested a prototype that functions at 850 nm.

The all-fiber analysis scheme is illustrated in Fig. 5b). This approach uses a FONT in-fiber single-mode splitter to split the signal. We found it necessary to manually twist the input and output leads of the splitter to prevent linear birefringence accumulation in these fibers.

The splitter achieves nearly 50/50 coupling with slightly greater than 3 dB insertion loss, and does not demonstrate noticeable polarization dependence.

The outputs of the splitter are each coupled into a Chiral Photonics in-fiber polarizer. The insertion loss of these polarizers is a 3-4 dB and the extinction ratio is greater than 20 dB.

In order to measure quadrature encoded data, the relative angle of the polarizers must be approximately 45°. To achieve this, we imparted a twist on the leads between the splitter and polarizers. In theory twisting one lead roughly 315° clockwise and the other roughly 315° counter-clockwise will ensure that light incident on the polarizers will be 0.073*660°=46° relative to each other. In practice, we find there is usually some intrinsic circular birefringence in the fiber, and it is simpler to twist one lead slightly and fix it, then twist the other and monitor the output until the desired relative angle is achieved.

The all-fiber solution sacrifices the functionality of the half-wave plate. The half-wave plate is used to rotate the plane-of-polarization of light entering the optics assembly, which allows us to verify both the amplitude of the photodetector response and the degree of linearity of light exiting the sensor fiber. In the all-fiber solution, we instead manually twist the connector interface between the PM fiber and the twisted SM sensing fiber. This effectively rotates the light incident on the twisted SM fiber by the angle of the twist, and rotates the light incident on the optics assembly by (1-*g*) multiplied by the angle of the twist. Manually twisting this interface by slightly over ±90° results in a complete Lissajous pattern,

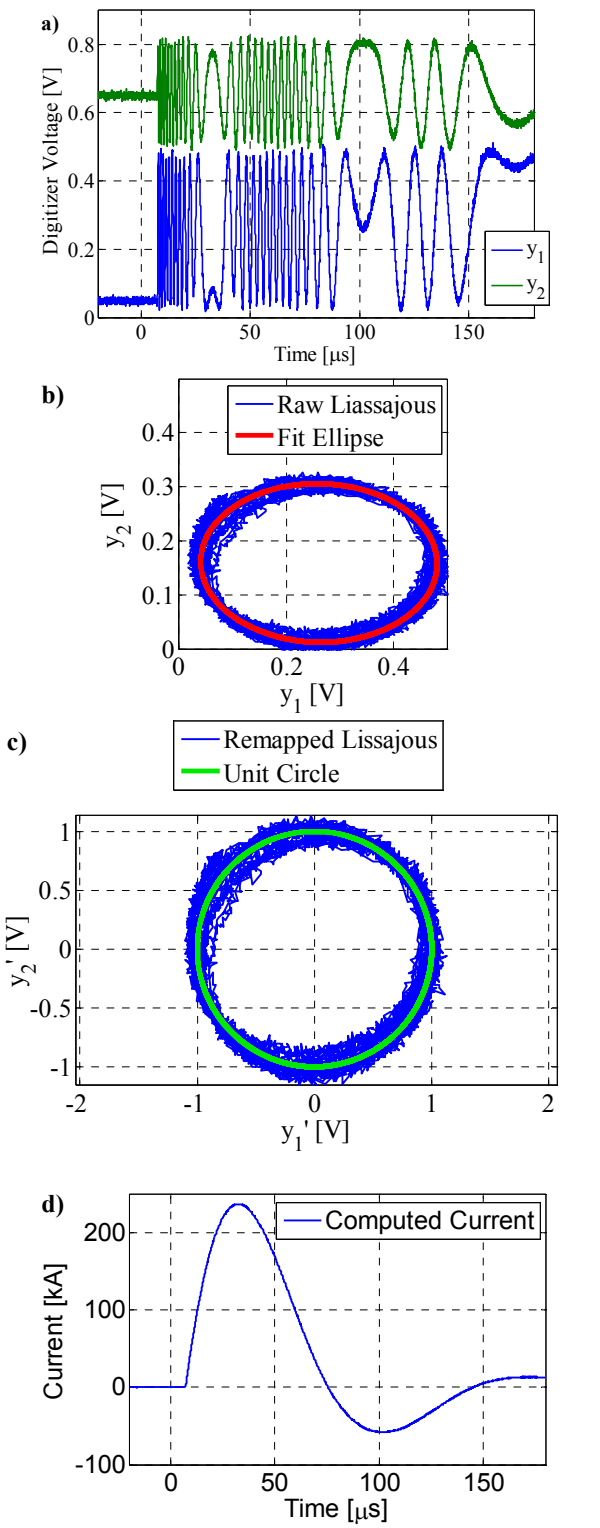

Figure 6. Data analysis process: a) raw digitizer data versus time; plotting the amplitudes of y_1 vs y_2 produces b) the raw Lissajous figure and elliptical fit; applying parameters from the elliptical fit to the raw Lissajous produces c) the re-mapped Lissajous figure; d) current computed from re-mapped data in c) using Eq. (1) and Eq. (3).

which provides the amplitude and polarization information necessary to assess diagnostic performance.

B. Data Analysis

A complete description of our preferred method of data analysis is beyond the scope of this paper [5]. A summary follows.

We orient our polarizers at relative angles of near 45°. Linear birefringence is sometimes unavoidable in the fiber lengths leading to and from the sensor fiber, which may degrade the linearity of the light incident on the sensing region and introduce retardation at the sensor fiber output, causing the Lissajous to take the form of a tilted ellipse, with minima that are offset from zero.

We use a direct least-squares fit to calculate parameters of the elliptical Lissajous recorded during experiment, then use those parameters to re-map the measured data to a unit circle. We then take the arc-tangent of the re-mapped data as a function of time. Boolean logic is used to handle instances where the rotation exceeds 2π.

It can be shown [5] that the arc-tangent of the re-mapped data is related to the angle of rotation of the plane-of-polarization through:

$$\beta(t) = \frac{1}{2}\left(\pm\tan^{-1}\frac{y_2'(t)}{y_1'(t)} - \tan^{-1}\frac{y_2'(0)}{y_1'(0)}\right), \qquad (3)$$

where $\beta(t)$ is the angle of rotation of plane-of-polarization from Eq. (1), and $y_1'(t)$ and $y_2'(t)$ are the re-mapped channels of measured data. In practice, there is no ambiguity in the sign on the first arc-tangent term in Eq. (3)—it can be determined by considering the direction of propagation of light and relative polarizer angles.

$\beta(t)$ can be related to current through application of Eq. (1). The needed parameters to do so are N, the number of fiber loops, and μV, the Verdet constant.

We have found the NIST2 [6] model of Verdet constant to be in the best agreement with other diagnostics. Our computed currents from Faraday Effect sensors have systematically been greater than currents measured using other current diagnostics, by roughly 1.6% at 635 nm and 1.1% at 850 nm. Since this is better than the expected accuracy of the diagnostics with which we use for comparison, we continue to use the NIST2 model.

We have developed an algorithm that performs the aforementioned steps automatically. The only user inputs necessary are the wavelength of light and number of fiber loops N. The elliptical fit is direct, so no iteration is required and convergence is guaranteed.

An example of the algorithm execution is shown in Fig. 6.

B. Experimental Data

A Faraday Rotation sensor was installed at the output of a two-stage explosive flux compression generator, at a location indicated approximately in Figure 7. The purpose of the diagnostic was to monitor current at the output of the second stage of the generator.

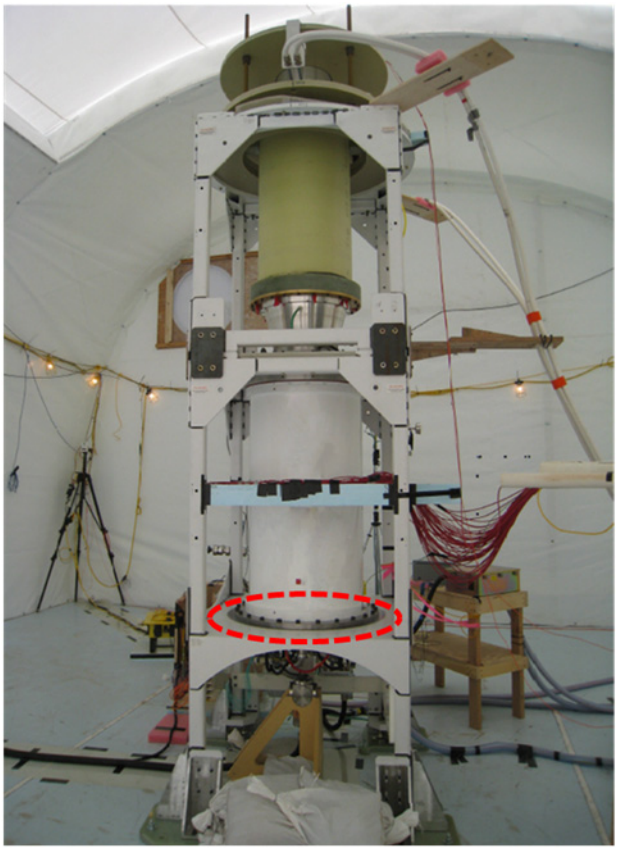

Figure 7. A photograph of the two-stage generator on the shot table. The approximate location of the Faraday Rotation sensor fiber is indicated by the dashed ellipse.

The generator is seeded with an initial current of 110 kA from a capacitor bank. The first stage of the generator is a helical generator. The peak current output of the helical generator is about 17 MA. The second stage is a coaxial generator. The peak current out of the coaxial generator is about 98 MA.

The sensor consisted of single-mode fiber twisted at a rate of 10 twists/m and looped approximately 1.049 times around an insulator at the generator output.

The layout of the diagnostic was similar to that shown in Fig. 5. The light source was an 850 nm battery driven diode laser, located in a bunker. The optical analysis hardware was placed on the shot table and destroyed with the experiment.

The details of the data analysis are very similar to those previously detailed and will therefore be omitted.

The analyzed data is shown in Fig. 8. In Fig. 8a), the current computed by analyzing the FRD data is compared with the average of two seed bank current monitors during seed bank operation, and the average of two opposite-polarity B-dot probes during late helical generator and coaxial generator operation. The B-dot probes, seed bank current monitors, and other associated instrumentation were calibrated prior to experiment. The agreement

between the Faraday Rotation data and other diagnostics is excellent. The dynamic range of the FRD is from less than 10 kA to near 100 MA, or greater than 80 dB. In Fig. 8b), the FRD measured current is compared with the same integrated B-dot probes near peak coaxial generator current. The Faraday Rotation fiber fails 2 microseconds before peak current, but agrees to within a percent of the B-dot probes prior to that.

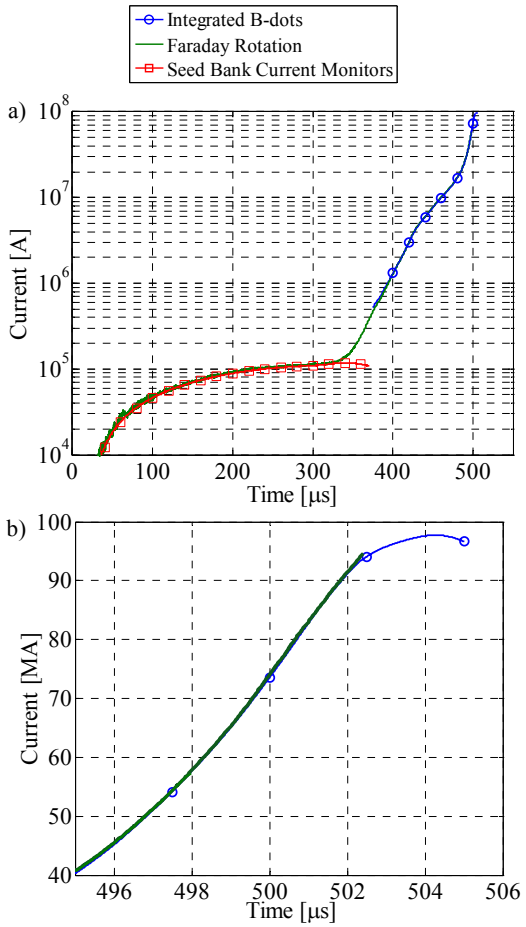

Figure 8. Current measured from the generator shown in Fig. 7. The current computed from the Faraday Rotation data is shown in a solid green line. The average of two calibrated integrated B-dot probe signals and the average of two capacitor bank current monitors are also shown.

IV. Summary

Fiber based FRDs offer a means of measuring pulsed currents with great immunity to EMI and noise, and excellent linearity in large magnetic fields. We have made simplifications to the hardware necessary to obtain quadrature-encoded data by developing an all-fiber analysis scheme. We have developed a numerical model that is a useful tool for quantifying deviation from ideal diagnostic performance prior to experiment. We have developed a method of data analysis that is automated, fast, and gives improved time resolution over many existing methods. Our experimental results agree well with other diagnostics.

V. ACKNOWLEDGEMENTS

The authors would like to thank Bruce Marshall and Lynn Veeser for their substantial and invaluable support.

VI. REFERENCES

[1] A. M. Smith, "Polarization and magneto-optic properties of single-mode optical fiber," *Appl. Opt. 5*, pp. 52-56, 1978.

[2] S. C. Rashleigh, "Origins and Control of Polarization Effects in Single-Mode Fibers," *Journal of Lightwave Technology*, vol. LT-1, no. 2, Jun. 1983.

[3] A. Simon, "Polarization optics of twisted single-mode fibers," *Applied Optics*, vol. 18, no. 13, pp. 2241-2251, Jul. 1979.

[4] A. Gerrard and J. M. Burch, *Introduction to Matrix Methods in Optics*. New York: Dover Publications, Inc, 1994, p. 212.

[5] A. D. White, G. B. McHale, and D. A. Goerz, "Faraday Rotation Data Analysis with Least-Sqaures Elliptical Fitting," *work in progress*.

[6] A. H. Rose, S. M. Etzel, and C. M. Wang, "Verdet Constant Dispersion in Annealed Optical Fiber Sensors," *Journal of Lightwave Technology*, vol. 15, no. 5, pp. 803-807, May 1997.